Research Paper

Cogging Force Reduction in PMLSMs Using Segmented Magnets

Naghi Rostami [*] , *Amjed A. Kadhim* , and *Mohammad Bagher Bannae Sharifian*

Faculty of Electrical and Computer Engineering, University of Tabriz, Tabriz, Iran.

Abstract— *Permanent Magnet Linear Synchronous Motors (PMLSMs) suffer from inevitable cogging force, especially in low-speed applications. In this paper, a new PMLSM is presented that uses segmented magnets instead of typically used rectangular magnets. This results in a significant reduction in cogging force and improved back EMF waveform. However, with these types of magnets, the actual three-dimensional (3D) structure of the machine cannot be reduced to a 2D problem because the thickness of the magnets varies with the depth of the device. Although 3D Finite Element Analysis (FEA) can be used, this method is very time-consuming even for one calculation step, which makes it difficult to use in optimization processes. To overcome these challenges, quasi-3D approach is used to transform the actual 3D structure of the machine into several 2D models and find the overall performance by combining the results obtained for each 2D problem. Genetic algorithm combined with quasi-3D method is used to find the appropriate thickness of each PM segment.*

Keywords—Permanent magnet linear motor, cogging force, segmented surfaced-mounted PMLSMs.

1. Introduction

Linear motors are used to directly convert electrical energy into translatory motion without using any intermediate mechanical means to convert rotary motion into linear motion. Among the different types of linear motors, Permanent Magnet Linear Synchronous Motors (PMLSMs) are widely used in industrial applications [1–4]. PMLSMs offer higher efficiency and power density compared to Linear Induction Motors (LIMs). According to [5, 6], power density and efficiency of a PMLSM are approximately 1.13 and 1.71 times higher than that of a LIM, respectively. Therefore, the higher cost of active materials used in PMLSMs can be amortized in a very short time with less electrical energy consumption [7]. However, one of the main disadvantages of the PMLSMs is the cogging force caused by the interaction between the magnets and iron core [8]. In [9, 10], thrust fluctuation caused by cogging force has been analysed for a new toroidal PMLSM. It has been shown that the cogging force significantly deteriorates the performance of the control system.

To avoid the negative effects of cogging force such as speed fluctuations, vibration and noise and problems in the drive system, it should be reduced. Many techniques have been proposed in the literature on how to reduce the cogging torque/force. A comprehensive review article on cogging force reduction methods in PM machines is presented in [11]. Cogging force/torque reduction techniques have been classified for both rotary and linear permanent magnet machines. Magnet/slot skewing, use of proper combination of slots and poles, selecting an appropriate magnet width, and determining proper slot opening width are some of

the methods used. Although the considered methods reduce the cogging, some of them greatly increase the complexity of the structure and construction costs, and may have adverse effects on other performance characteristics of the machine, such as the induced back-EMF waveform. Liu et al. [12], have proposed a method based on different combination of pole arc coefficient for interior PMSM. In [13], a new PMLSM with Halbach arrays has been presented to suppress thrust ripple. The slots of a PMLSM are shifted in [14] to reduce the cogging force. A new segmented-stator PMLSM has been proposed in [15] in which an appropriate slot-pole combination was selected and the relative position of the two stators was adjusted to mitigate the cogging force. In [16], a double-layer reverse skewed coil (DRSC) is employed to reduce the thrust ripple while increasing the output thrust. In [17], the geometric parameters of the PMLSM, such as tooth width and PM arc, have been determined in such a way that costs and cogging force are reduced. However, a constant PM width along the depth of the machine is used. The use of auxiliary teeth, narrowing the slot opening, and the use of arc shaped magnets are the three effective techniques that have been used in [18]. Although the cogging force is significantly reduced and the back-EMF waveform is closer to the ideal sine, the structure is more complicated and the cost of construction has increased. In [19], the optimal values of the main dimensions of a PMLSM are determined to reduce cogging force. PM width is kept constant and the method used is very time consuming. Wang et al. [20] presented a technique for fractional-slot PMLMs with double-layer concentrated windings, in which the cogging force was significantly reduced by adjusting the dimensions of the armature core along with the magnet skewing.

An analytical cogging force calculation based on the virtual work method is presented in [21]. However, simplifying assumptions have been used in the calculations which overshadow the accuracy of the results. In [22], the stator teeth were asymmetrically distributed to mitigate the cogging force. A time-consuming FEM was used to calculate the cogging force and back-EMF waveform, and no optimization was performed. In [23, 24], quasi-3D approach has been used to calculate the air-gap magnetic flux distribution and then the cogging torque of an Axial-Flux Permanent Magnet

(AFPM) machine. Based on this method, the AFPM machine structure is subdivided into a sufficient number of 2D models in the direction of the machine radius. In [25], the cogging force of a PMLSM was reduced by step-skewed stator cores. However, the machine structure has become more complicated. In [26], segmented PMs are used to reduce the cogging torque of an axial flux PM machine.

The PM segments are shifted relative to each other and the shift angle is optimized by Response Surface Methodology. However, no study has been done on the effect of using this method on other characteristics of the machine. It seems that the application of the method increases the harmonic content of the induced back-EMF. Regarding the modelling and analysis of electric machines, FEM is the most widely used method among others [27]. Although this method is well-established and provides high accuracy, the high computation time makes its use in iterative optimization processes or parametric studies almost impossible.

The produced cogging force changes with different relative magnet width (RMW). Both peak-to-peak value of the cogging force and its waveform change with the change of RMW. The idea of using segmented magnets comes from the fact that a combination of magnets with different RMW can minimize the produced resultant cogging. In this paper, as illustrated in Fig. 1, instead of commonly used rectangular PMs, segmented PMs with different RMW are used. It should be kept in mind that RMW also affects other quantities of the machine such as the air-gap flux density distribution, and the induced back-EMF waveform. Therefore, the width of each segment is optimized using genetic algorithm to reduce cogging force and make the back-EMF waveform as close as possible to an ideal sine. Due to the many repeated calculations in the optimization process, a fast but accurate enough 2D analytical method is used in combination with quasi-3D approach.

The main contributions of this article can be expressed in two parts. First, introducing new segmented magnets that have been used instead of rectangular magnets where after optimizing the thickness of each segment, the cogging force has been significantly reduced and the back EMF waveform has been significantly improved. Second, presenting a method based on quasi-3D approach that, by converting the 3D structure of the machine into several 2D problems, provides a fast and accurate solution to calculate the air gap flux density distribution and thereby the cogging force, which is suitable to be used in the optimization process.

2. ANALYTICAL METHOD

2.1. Quasi-3D approach

According to [28, 29], more favorable performance characteristics such as suppressed cogging and almost sinusoidal back-EMF waveform can be achieved by using magnets with a more complex outline, such as sinusoidal magnets. The problem however is that magnets are hard and brittle which makes their shaping difficult and increases the possibility of cracks under mechanical impacts. Although better mechanical strength can be provided by magnets bonded with polymer materials, but this reduces the properties of magnets [23], [30]. This is why rectangular magnets are used in most of PMLSMs. However, the produced air-gap magnetic field by rectangle PMs is nearly rectangular and contains many harmonics, which in turn makes the back-EMF waveform far from sinusoidal, and the existing harmonic components cause thrust ripple even with pure sinusoidal current feeding into the winding.

To find an intermediate solution and taking into account the practical limitations, segmented-magnets can be used that divides each pole magnet into several rectangular segments with different widths. In rectangular magnets, magnet width is constant with respect to the machine depth. Therefore, a 2D FEA can be performed. However, by using segmented magnets instead of
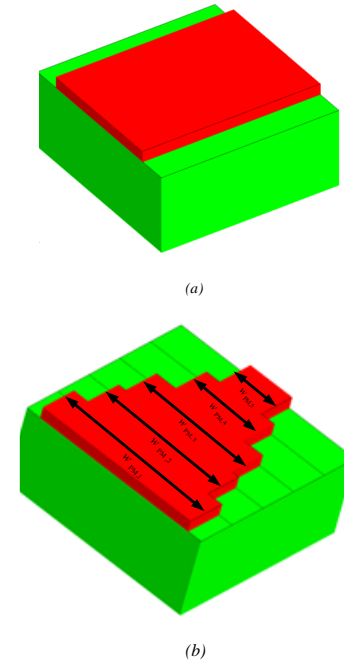

(a)

(b)

Fig. 1. Surface-mounted permanent magnets on mover back-iron; (a) Commonly used rectangular PMS, (b) Segmented PMs with different relative magnet width (magnet width to pole pitch ratio PMLSM).

rectangular ones, the results are no longer accurate using 2D FEA. Besides, 3D FEA is very time consuming and difficult to apply, especially when the goal is to obtain optimal dimensions. To solve this problem, as illustrated in Fig. 2, quasi-3D approach is used, in which the 3D structure of the machine is divided into 2D problems by the number of segments, and the overall characteristics of the machine are obtained by combining the results.
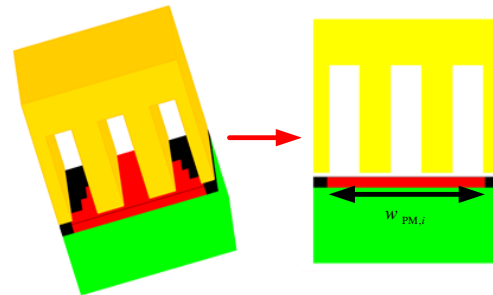

Fig. 2. Converting the 3D geometry of PMLSM equipped with segmented magnets to 2D models using quasi-3D computation method. The number of 2D models is equal to the number of segments. $W_{PM,i}$ is the width of the magnet in the ith segment.

2.2. 2D analytical magnetic field calculations

After dividing the actual 3D structure of the machine into several 2D models, a 2D analytical model is created to calculate the air-gap flux density distribution and consequently to calculate the cogging force and induced back-EMF. To simplify the problem, a set of assumptions is considered. It is assumed that the PLMSM is symmetrical along z direction in each layer and therefore the problem is converted to 2D models with the number of PM segments. Magnetic vector potential has only z component because it is assumed that the magnetic flux density and the magnetic field intensity vector have only x and y components. Relative permeability of rotor/stator irons is assumed to be infinite.

The general graphical structure of each 2D model and its main parameters are illustrated in Fig. 3.
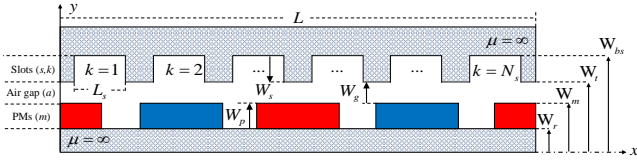

Fig. 3. Representation of spatial parameters and subdomains of PMLSM with surface mounted magnets.

A) Governing partial differential equations [31, 32]

Magnetic flux density **B** caused only by the magnets is calculated by the following steps;

- The model is divided into sub-regions considering their magnetic properties. Region I includes air-gap area and slots areas while the region II is denotes to PM region.
- The governing partial differential equations (PDEs) are written for each sub-region. In region I, the magnetic vector potential A_z meets Laplace's equations while in region II, Poisson's equations is satisfied as follows;

$$\frac{\partial^2 A_{zI}}{\partial x^2} + \frac{\partial^2 A_{zI}}{\partial y^2} = 0 \qquad \text{for region I,}$$
$$\frac{\partial^2 A_{zII}}{\partial x^2} + \frac{\partial^2 A_{zII}}{\partial y^2} = \mu_0 \left(\frac{\partial M_x(x)}{\partial x} - \frac{\partial M_y(x)}{\partial x} \right) \quad \text{for region II.} \tag{1}$$

- Then **B** can be written in terms of magnetic vector potential $\mathbf{A} = [0, 0, A_z(x,y)]$ as:

$$\mathbf{B} = \nabla \times \mathbf{A}$$
$$[B_x(x,y), B_y(x,y), 0] = \left[\frac{\partial A_z(x,y)}{\partial y}, \frac{-\partial A_z(x,y)}{\partial x}, 0 \right]. \tag{2}$$

where superscripts I and II denote to region I and region II, respectively. $M_x(x)$ and $M_y(x)$ respectively represent the tangential and perpendicular components of the magnetization intensity vector in any position x along the machine length which depends on the magnetization pattern of the magnets. To put it better, in Cartesian coordinate system, the magnetization vector of the magnet area can be expressed as:

$$\mathbf{M} = M_x(x)\hat{a}_x + M_y(x)\hat{a}_y. \tag{3}$$

where $\hat{a}_x$ and $\hat{a}_y$ are the unit vectors in the tangential and perpendicular directions. In this study, the magnetization is only in $\hat{a}_y$ direction. The distribution of magnetization, illustrated in Fig. 4, can be expressed with Fourier series expansion as:
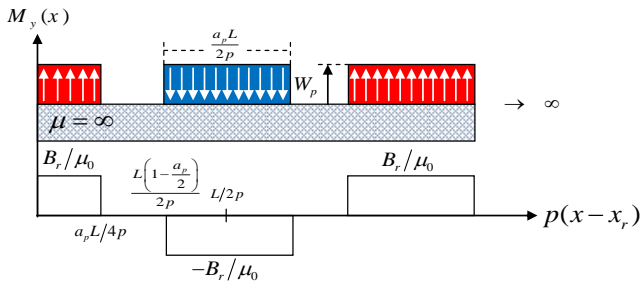

Fig. 4. Perpendicular magnetization pattern. Note that tangential component is zero.

$$M_y(x) = \sum_{n=1}^{\infty} M_{yn} \cos\left(\frac{n\pi p}{L/2}(x - x_r) \right), \tag{4}$$

$$M_{yn} = \frac{2B_r}{\mu_0 n\pi} \left[\sin\left(n\pi/2 \right) + \sin\left(n\pi(1 - \frac{a_p}{2}) \right) \right], \tag{5}$$

$$M_x(x) = 0. \tag{6}$$

where B_r is the PM remnant flux density, a_p is the relative magnet width which is a different value for each segment in this study. L is the mover length. M_{yn} is the nth element of the perpendicular components of the magnetization vector, $x_r = vt + x_{r0}$ is the mover position. v and x_{r0} are the mover linear speed and its initial position, respectively.

To achieve an analytical solution, PDEs are first obtained for each sub-region, and then the homogenous and particular solutions are determined so that the boundary conditions are satisfied. Therefore, it is necessary to determine the boundary conditions carefully.

B) Boundary conditions

Determining the boundary conditions is necessary to calculate the PDEs and determine the integration constants. According to continuous boundary condition, the perpendicular component of magnetic flux density vector B_y is continuous at the interface between two adjacent areas. Also, the tangential component of magnetic field intensity vector H_x is continuous at the interface between two adjacent areas in the absence of any surface current density. Furthermore, according to Neumann boundary condition, the tangential component of magnetic field intensity vector H_x at the surface adjacent to area with infinite permeability is zero.

Considering the mentioned boundary conditions, for the considered PMLSM with surface-mounted PMs on the mover back-iron, the following boundary conditions can be written on the interface of each area with adjacent area. Eq. (7) states that the tangential component of the magnetic field intensity vector at the interface between the magnets and the mover core with infinite permeability is zero. Also, Eqs. (8) and (9) respectively state that the perpendicular components of the magnetic flux density vector and the tangential component of the magnetic field intensity vector are equal at the interface between the air-gap and magnets.

$$H_x^m(x,y) \Big|_{=W_r} = \frac{1}{\mu_0 \mu_r} \frac{\partial A_z^m(r,\theta)}{\partial y} \Big|_{=W_r} = 0, \tag{7}$$

$$B_y^m(x,y)\big|_{y=W_m} = B_y^a(x,y)\big|_{y=W_m}, \tag{8}$$

$$H_x^m(x,y)\big|_{y=W_m} = H_x^a(x,y)\big|_{y=W_m}. \tag{9}$$

Furthermore, the perpendicular component of magnetic field intensity H_y at both sides of each slot should be zero (Eq. (10)). At the interface between air gap and opening of the slots, the perpendicular component of magnetic flux density vector B_y and tangential component of magnetic field intensity vector H_x should be continuous (Eqs. (11)-(12)). Also, at the bottom of each slot, the tangential component of magnetic field intensity vector is zero (Eq. (13)).

$$H_y^s(x,y) \Big|_{=x_{ck} \pm \frac{a_s L}{2Ns}} = \frac{-1}{\mu_0} \frac{\partial A_z^s(x,y)}{\partial x} \Big|_{=x_{ck} \pm \frac{a_s L}{2Ns}} = 0. \tag{10}$$

$$B_y^a(x,y)\big|_{y=W_t} = B_y^s(x,y)\big|_{y=W_t}. \tag{11}$$

$$H_x^a(x,y)\Big|_{y=W_t} = \begin{cases} \sum_{k=1}^{\infty} H_x^s(x,y)\Big|_{y=W_t} & x_c^k - L_s \le x \le x_c^k + L_s \\ 0 & \text{Otherwise} \end{cases}$$
$$L_s = \frac{a_s L}{2N_s}, x_c^k = \frac{L}{2N_s}(1-a_s)$$
$$+ \frac{L_s}{2} + (k-1)Ls \quad k = 1,2,...,N_s, \tag{12}$$

$$H_x^s(x,y)\Big|_{=W_{bs}} = \frac{1}{\mu_0}\frac{\partial A_z^s(x,y)}{\partial y}\Big|_{=W_{bs}} = 0. \tag{13}$$

where x_c^k is the position of the center of kth slot in the direction of x.

C) Air gap magnetic flux density and cogging force calculation

By solving the governing partial differential equations for each region, the perpendicular and tangential components of the air gap magnetic flux density can be expressed as:

$$B_y^a(x,y) = \sum_{n=1}^{N}\left\{\frac{2n\pi}{L}\left[a_n^a e^{\frac{2n\pi}{L}W_{gm}} + b_n^a e^{\frac{-2n\pi}{L}W_{gm}}\right] \times \sin\left(\frac{2n\pi}{L}x\right)\right.$$
$$\left. + \frac{2n\pi}{L}\left[c_n^a e^{\frac{2n\pi}{L}W_{gm}} + d_n^a e^{\frac{-2n\pi}{L}W_{gm}}\right] \times \cos\left(\frac{2n\pi}{L}x\right)\right\}, \tag{14}$$

$$B_y^a(x,y) = \sum_{n=1}^{N}\left\{\frac{2n\pi}{L}\left[a_n^a e^{\frac{2n\pi}{L}W_{gm}} + b_n^a e^{\frac{-2n\pi}{L}W_{gm}}\right] \times \sin\left(\frac{2n\pi}{L}x\right)\right.$$
$$\left. + \frac{2n\pi}{L}\left[c_n^a e^{\frac{2n\pi}{L}W_{gm}} + d_n^a e^{\frac{-2n\pi}{L}W_{gm}}\right] \times \cos\left(\frac{2n\pi}{L}x\right)\right\}. \tag{15}$$

where N and U are the number of harmonics of the general solutions in region I and region II, respectively. W_{gm} is the middle width of the air gap region. Unknown integration constants are calculated by applying the boundary conditions stated.

The produced cogging force at each computational plane is computed as:

$$F_{cog,i}(x) = \frac{d_{zi}}{\mu_0}\int_0^L B_{x,i}B_{y,i}dx. \tag{16}$$

where d_{zi} is the thickness of ith PM segment in the direction of z-axis. The total cogging force is given by:

$$F_{cog}(x) = \sum_{i=1}^{N} F_{cog,i}(x). \tag{17}$$

3. DESIGN OPTIMIZATION AND RESULT DISCUSSION

Genetic algorithm is implemented to reduce EMF harmonics and cogging force of the considered PMLSM. The width of each PM segment (here 5 segments) is considered as the optimization parameters to be determined through an iterative process. For all candidate solutions, which are updated iteratively, the fitness values are calculated and finally the population of strings with the highest fitness is selected. The objective function is the combination of the produced cogging force (peak-to-peak) and the THD of induced EMF. In each iteration, a population of optimization parameters is imported from genetic algorithm to quasi 3-D design program. Quasi-3D method converts the 3D model into five 2D models, and then the cogging force and induced back-EMF waveform are calculated by the analytical method mentioned above.

The considered machine is a single-sided PMLSM with the main parameters listed in Table 1. After optimization, the relative magnet width of five PM segments is obtained as 0.85, 0.69, 0.61, 0.39, and 0.24, respectively. The average value of RMWs is 0.556, which is a small value and it is not possible to achieve acceptable

Table 1. The main parameters of the considered PMLSM.

Explanation	Value	Unit
Linear speed	1	m/s
Thickness of the mover back-iron	0.028	(m)
Height of PMs	0.004	(m)
Air-gap length	0.0015	(m)
Height of the slots	0.040	(m)
Total length of the motor	0.819	(m)
Remanent flux density of the PM material	1.05	(T)
Number of stator slots	36	-
Number of pole pairs	6	-
Slot width to slot pitch ratio	0.5	-

performance characteristics with a rectangular magnet with this RMW. Therefore, it can be concluded that this design has also led to a significant reduction in the amount of expensive magnets used.

The cogging force produced by each individual rectangular PM segment and the cogging force produced by the proposed PM arrangement are shown in Fig. 5. As it is obvious, the cogging force produced by the sections with relative magnet widths of 0.61 and 0.69 have values with the opposite sign to segments with relative magnet widths of 0.24, 0.39, and 0.85. Therefore, the cogging force produced by one segment can cancel the cogging produced by the other segment, which in turn leads to a drastic reduction in the resulting cogging. For example, in electrical angle of 15 degree, the cogging force values corresponding to each segment (from the smallest RMW to the largest RMW) are equal to -418.2, -226.8, +559.7, +470.7, and -383.2 respectively. Then the net cogging force using quasi-3D approach is (-418.2-226.8+559.7+470.7-383.2)/5=0.44.
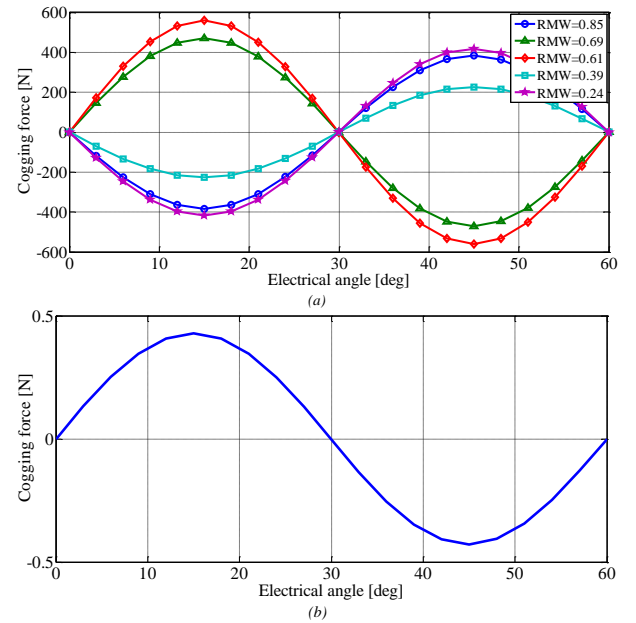

Fig. 5. Cogging force waveform; (a) Cogging force produced by each individual rectangular PM segment, (b) Cogging force produced by proposed PM arrangement.

The same argument is true for induced back-EMF. As illustrated in Fig. 6, the back-EMF waveform induced by rectangular PMs contains many harmonic components and is far from a sinusoidal waveform for almost all RMWs. Whereas, if these rectangular magnets are replaced with the arrangement shown in Fig. 1, the harmonic components of the back EMF induced by one segment are attenuated by the back EMF induced by the other segment, leading to an improvement in the resulting EMF waveform. As it is clear from Fig. 7, the resulting induced back-EMF waveform

is closer to a sine wave and the harmonic contents are greatly reduced. It is worth mentioning that the goal of optimization is to improve the back-EMF along with reducing the cogging. This is why the back-EMF waveform still has harmonic contents, albeit small.
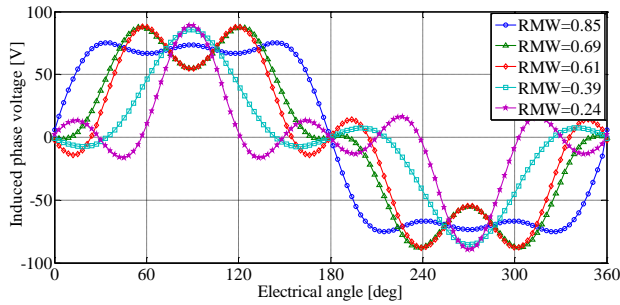

Fig. 6. The back-EMF waveform induced by each individual rectangular PM in the considered PMLSM.
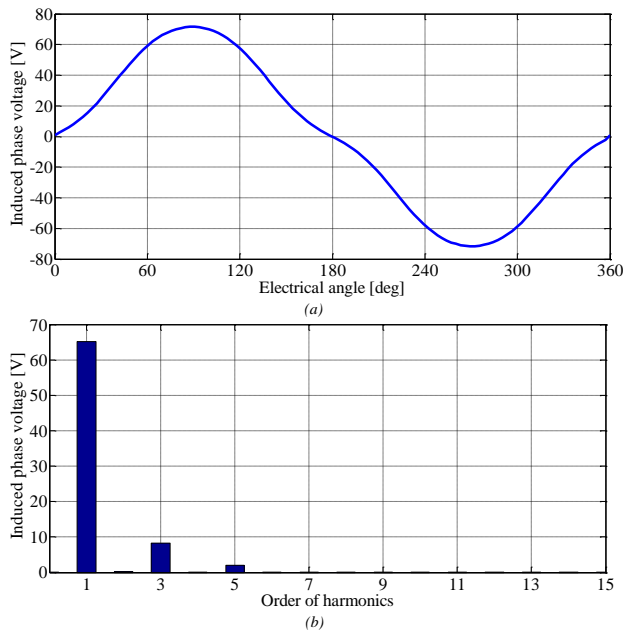

Fig. 7. The induced back-EMF waveform and its harmonic contents for the PMLSM with proposed segmented PM arrangement ; (a) Induced back-EMF waveform , (b) Harmonic contents of the EMF.

4. CONCLUSION

A new segmented magnet arrangement was presented, which, if replaced with rectangular magnets, causes a significant reduction in cogging force and a significant improvement in the back EMF waveform. Since the produced cogging force and induced back EMF are strongly influenced by the relative magnet width, the idea comes to mind that a combination of magnets with different widths can cancel each other's cogging, resulting in less resultant cogging. A similar argument can be made regarding back EMF waveform improvement. However, the width of each magnet segment must be precisely determined, which requires a fast and accurate enough analytical method to be adopted within an optimization program. Therefore, a quick but sufficiently accurate 2D analytical method combined in quasi-3D approach is used to predict air gap magnetic flux density, cogging force and back EMF wave form in a flat single-sided PMLSM. After optimization by genetic algorithm, the relative magnet width for each segment is

obtained as 0.85, 0.69, 0.61, 0.39, and 0.24, respectively which has the average value of 0.556. The results show that by using segmented magnets, a significant reduction in the cogging force and a notable improvement in the back EMF waveform have been achieved even with a lower amount of magnet used.

REFERENCES

[1] J. Qian, L. Bao, C. Ji, and J. Wu, "Magnetic field modeling and analysis for permanent magnet synchronous linear motors," *Int. J. Appl. Electromagn. Mech.*, vol. 60, no. 2, pp. 209–221, 2019.

[2] R. Cao, Y. Jin, M. Lu, and Z. Zhang, "Quantitative comparison of linear flux-switching permanent magnet motor with linear induction motor for electromagnetic launch system," *IEEE Trans. Ind. Electron.*, vol. 65, no. 9, pp. 7569–7578, 2018.

[3] F. Cui, Z. Sun, W. Xu, W. Zhou, and Y. Liu, "Comparative analysis of bilateral permanent magnet linear synchronous motors with different structures," *CES Trans. Electr. Mach. Syst.*, vol. 4, no. 2, pp. 142–150, 2020.

[4] Z. He, F. Dong, J. Zhao, L. Wang, J. Song, Q. Wang, and X. Song, "Thrust ripple reduction in permanent magnet synchronous linear motor based on tuned viscoelastic damper," *IEEE Trans. Ind. Electron.*, vol. 66, no. 2, pp. 977–987, 2018.

[5] O. Taskin, *Design and implementation of a double-sided coreless linear motor*. PhD thesis, Thèse de doctorat, Istanbule Technical University Graduate School of Science . . . , 2015.

[6] J. G. Hayes and G. A. Goodarzi, "Electric powertrain: energy systems, power electronics and drives for hybrid, electric and fuel cell vehicles," 2018.

[7] M. Torrent, J. I. Perat, and J. A. Jiménez, "Permanent magnet synchronous motor with different rotor structures for traction motor in high speed trains," *Energies*, vol. 11, no. 6, p. 1549, 2018.

[8] G. Meng, Y. Yuan, Y. Sun, H. Liu, and Z. Zhu, "A novel method to reduce of cogging force in a linear flux-switching permanent magnet brushless ac machine," *J. Electr. Eng. Technol.*, vol. 14, pp. 653–662, 2019.

[9] R. Zeng, J. Zhao, S. Yan, and Y. Mao, "Research on cogging force suppression for toroidal pmlsm based on disturbance observer," *CES Trans. Electr. Mach. Syst.*, 2023.

[10] M. Sumega, P. Rafajdus, and M. Stulrajter, "Current harmonics controller for reduction of acoustic noise, vibrations and torque ripple caused by cogging torque in pm motors under foc operation," *Energies*, vol. 13, no. 10, p. 2534, 2020.

[11] W. Hao, G. Zhang, W. Liu, H. Liu, and Y. Wang, "Methods for reducing cogging force in permanent magnet machines: A review," *Energies*, vol. 16, no. 1, p. 422, 2022.

[12] F. Liu, X. Wang, Z. Xing, A. Yu, and C. Li, "Reduction of cogging torque and electromagnetic vibration based on different combination of pole arc coefficient for interior permanent magnet synchronous machine," *CES Trans. Electr. Mach. Syst.*, vol. 5, no. 4, pp. 291–300, 2021.

[13] X. Xu, Z. Sun, B. Du, and L. Ai, "Pole optimization and thrust ripple suppression of new halbach consequent-pole pmlsm for ropeless elevator propulsion," *IEEE Access*, vol. 8, pp. 62042–62052, 2020.

[14] X. Huang, T. Ji, L. Li, B. Zhou, Z. Zhang, D. Gerada, and C. Gerada, "Detent force, thrust, and normal force of the short-primary double-sided permanent magnet linear synchronous motor with slot-shift structure," *IEEE Trans. Energy Convers.*, vol. 34, no. 3, pp. 1411–1421, 2019.

[15] W. Li and T. Ching, "A new segmented-stator linear vernier permanent magnet machine for direct-drive applications," in *2017 IEEE Int. Electr. Mach. Drives Conf. (IEMDC)*, pp. 1–6, IEEE, 2017.

[16] W. Wang, J. Zhao, J. Song, F. Dong, K. Zong, and G. Li, "Thrust performance improvement for pmslm through double-layer reverse skewed coil and wrf-mkh method," *IEEE/ASME Trans. Mechatron.*, vol. 25, no. 6, pp. 2950–2960, 2020.

[17] C. Deng, C. Ye, J. Yang, S. Sun, and D. Yu, "A novel permanent magnet linear motor for the application of electromagnetic launch system," *IEEE Trans. Appl. Supercond.*, vol. 30, no. 4, pp. 1–5, 2020.

[18] S. Jiang, P. Ye, G. Jin, Y. Qi, and H. Lin, "Optimization design to reduce detent force and standardize back-emf for permanent magnet synchronous linear motor," in *IECON 2016-42nd Annu. Conf. IEEE Ind. Electron. Soc.*, pp. 1716–1720, IEEE, 2016.

[19] J. A.-K. Mohammed, F. M. Mohammed, and A. A. Raghda'a Ahmed, "Design and optimization of a surface-mounted permanent-magnet linear synchronous motor with maxwell ansys," *Al-Khwarizmi Eng. J.*, vol. 15, no. 3, pp. 1–15, 2019.

[20] Q. Wang, B. Zhao, J. Zou, and Y. Li, "Minimization of cogging force in fractional-slot permanent magnet linear motors with double-layer concentrated windings," *Energies*, vol. 9, no. 11, p. 918, 2016.

[21] M. Rusli, I. N. G. Wardana, M. A. Choiron, and M. A. Muslim, "Investigation of cogging forces using reluctance circuits equivalent approximation in a ladder secondary single-sided linear induction motor," *East.-Eur. J. Enterp. Technol.*, no. 2 (5), pp. 23–35, 2019.

[22] Q. Liu, H. Yu, M. Hu, C. Liu, J. Zhang, L. Huang, and S. Zhou, "Cogging force reduction of double-sided linear flux-switching permanent magnet machine for direct drives," *IEEE Trans. Magn.*, vol. 49, no. 5, pp. 2275–2278, 2013.

[23] N. Rostami and M. Rostami, "Analysis of afpm machines with cylindrically shaped magnets using quasi-3d method," *COMPEL - Int. J. Comput. Math. Electr. Electron. Eng.*, vol. 36, no. 4, pp. 1168–1183, 2017.

[24] A. H. Sharifi, S. M. Seyedi, and A. S. Mobarakeh, "Quasi-3d analytical prediction for open circuit magnetic field of axial flux permanent-magnet machine," in *Fundam. Res. Electr. Eng.: Sel. Pap. First Int. Conf. Fundam. Res. Electr. Eng.*, pp. 533–548, Springer, 2019.

[25] W. Hao and Y. Wang, "Comparison of the stator step skewed structures for cogging force reduction of linear flux switching permanent magnet machines," *Energies*, vol. 11, no. 8, p. 2172, 2018.

[26] S. Arand, "Optimization of pm segments shift angles for minimizing the cogging torque of yasa-afpm machines using response surface methodology," *J. Oper. Autom. Power Eng.*, vol. 9, no. 3, pp. 203–212, 2021.

[27] D. Habibinia, M. Feyzi, and N. Rostami, "A new method for computation of axial flux permanent magnet synchronous machine inductances under saturated condition," *J. Oper. Autom. Power Eng.*, vol. 6, no. 2, pp. 208–217, 2018.

[28] H. Tiegna, Y. Amara, and G. Barakat, "Validity domain of a quasi-3d multislice analytical model for synchronous axial flux machines with trapezoidal magnets," *Eur. Phys. J. Appl. Phys.*, vol. 70, no. 1, p. 10902, 2015.

[29] L. Jing, W. Tang, T. Wang, T. Ben, and R. Qu, "Performance analysis of magnetically geared permanent magnet brushless motor for hybrid electric vehicles," *IEEE Trans. Transp. Electrif.*, vol. 8, no. 2, pp. 2874–2883, 2022.

[30] T. N. Lamichhane, L. Sethuraman, A. Dalagan, H. Wang, J. Keller, and M. P. Paranthaman, "Additive manufacturing of soft magnets for electrical machines—a review," *Mater. Today Phys.*, vol. 15, p. 100255, 2020.

[31] F. Cui, Z. Sun, W. Xu, W. Zhou, and Y. Liu, "Comparative analysis of bilateral permanent magnet linear synchronous motors with different structures," *CES Trans. Electr. Mach. Syst.*, vol. 4, no. 2, pp. 142–150, 2020.

[32] X. Liu, J. Gao, S. Huang, and K. Lu, "Magnetic field and thrust analysis of the u-channel air-core permanent magnet linear synchronous motor," *IEEE Trans. Magn.*, vol. 53, no. 6, pp. 1–4, 2017.